nature physics

ARTICLES

https://doi.org/10.1038/s41567-020-0950-5

# Hidden magnetism at the pseudogap critical point of a cuprate superconductor

Mehdi Frachet[1,9], Igor Vinograd[1,9], Rui Zhou[1,2], Siham Benhabib[1], Shangfei Wu[1], Hadrien Mayaffre[1], Steffen Krämer[1], Sanath K. Ramakrishna[3], Arneil P. Reyes[3], Jérôme Debray[4], Tohru Kurosawa[5], Naoki Momono[6], Migaku Oda[5], Seiki Komiya[7], Shimpei Ono[7], Masafumi Horio[8], Johan Chang[8], Cyril Proust[1], David LeBoeuf[1]✉ and Marc-Henri Julien[1]✉

**The nature of the pseudogap phase of hole-doped cuprate superconductors is still not understood fully. Several experiments have suggested that this phase ends at a critical hole doping level $p^\star$, but the nature of the ground state for lower doping is still debated. Here, we use local nuclear magnetic resonance and bulk ultrasound measurements to show that, once competing effects from superconductivity are removed by high magnetic fields, the spin-glass phase of $La_{2-x}Sr_xCuO_4$ survives up to a doping level consistent with $p^\star$. In this material, the antiferromagnetic-glass phase extends from the doped Mott insulator at $p = 0.02$ up to $p^\star \approx 0.19$, which provides a connection between the pseudogap and the physics of the Mott insulator. Furthermore, the coincidence of the pseudogap boundary with a magnetic quantum phase transition in the non-superconducting ground state has implications for the interpretation of other experiments, particularly for transport and specific-heat measurements in high magnetic fields.**

Extensive studies of cuprate superconductors[1,2] have shown that, after three-dimensional Néel order disappears upon hole doping ($p$), there are still remnants of spin order at low temperature ($T$) in the form of a glass-like freezing of incommensurate antiferromagnetic correlations[3–9]. However, the importance of the coexistence of incommensurate spin order with superconductivity has been unclear. The glass-like characteristics and material-dependent phase boundaries of this 'antiferromagnetic glass' suggests that it is favoured by disorder[10,11], and that it is not unequivocally connected to either charge order, the pseudogap phase or superconductivity.

In $La_{2-x}Sr_xCuO_4$, the antiferromagnetic glass is favoured by charge-stripe (uniaxial charge-density wave) ordering at around $p=x=0.12$ and is clearly observed up to a maximum doping $p_{sg}\approx 0.135$ (Fig. 1)[3,4,6]. The persistence of spin freezing up to $p^\star\approx 0.19$ in samples doped with planar impurities has led to the hypothesis that the ground state of the pseudogap regime is an antiferromagnetic glass[6] and that antiferromagnetic correlations exist only below $p^\star$; that is, within the pseudogap phase[12]. However, the results on which this hypothesis is based are controversial[7] and their interpretation is debatable, as the introduction of impurities in the $CuO_2$ planes, while weakening superconductivity, also favours the freezing of antiferromagnetic fluctuations in the normal state[13,14]. Furthermore, a model in which glassy freezing is connected with the pseudogap faces difficulties, among which are the persistence of antiferromagnetic correlations above $p^\star$ (ref. [15]) and the disappearance of spin freezing well below $p^\star$ in most cuprates ($p_{sg}=0.08$ in $YBa_2Cu_3O_y$ (refs. [8,9])).

Here, we follow a different approach, without planar-impurity doping, to shed light on these fundamental issues. When superconductivity is quenched with high magnetic fields, we find that the antiferromagnetic glass of $La_{2-x}Sr_xCuO_4$ extends from the weakly doped insulator up to the pseudogap boundary $p^\star$. Specifically, previous neutron scattering studies showed that a magnetic field $B$ enhances static magnetism for $p\approx 0.10$–$0.12$ and even induces it for $p\approx 0.145$ (refs. [16–18]), but not at higher doping at which only the finite-energy spectrum is affected[19,20]. Here, using much higher field strengths, we discover that static or quasi-static magnetism actually persists well above $p\approx 0.145$ but not across the whole phase diagram; in fact, only up to a doping value consistent with $p^\star\approx 0.19$, the critical doping of the pseudogap phase.

To provide a benchmark for measurements near $p^\star$, we first report $^{139}$La nuclear magnetic resonance (NMR) and ultrasound results for the doping $p=0.148$ at which magnetism should be field dependent[16–18] (see Methods for experimental and sample details). Glassy freezing is typically seen in NMR as a broad peak in the nuclear spin-lattice relaxation rate $1/T_1$ versus $T$, when the inverse correlation time of spin fluctuations $\tau_c^{-1}$ matches the NMR frequency $\omega_{NMR} \sim 10^1$–$10^2$ MHz (refs. [5,9,21–24]). Such a peak, defining a freezing temperature $T_f$ at the NMR timescale, is seen in our high-field data and disappears at low fields (Fig. 2). The spatial heterogeneity that typifies spin glasses in $La_{2-x}Sr_xCuO_4$ with $x < 0.135$ (refs. [21–24]) is also present here, as shown by the large distribution of $T_1$ values (see Methods and Extended Data Fig. 1).

Our high-field ultrasound data (Fig. 2) also indicate the presence of a spin-glass state: a softening (decrease) in the sound velocity $\Delta v/v$, followed by a hardening (increase), is observed upon cooling, as in canonical spin glasses (see ref. [25] and Extended Data Fig. 2 for more details). Unlike in NMR, the temperature $T_{min}$ at which the sound velocity is minimum is not simply defined as the temperature at which $\tau_c^{-1}$ matches the ultrasound frequency. In fact, the

[1]Université Grenoble Alpes, INSA Toulouse, Université Toulouse Paul Sabatier, EMFL, CNRS, LNCMI, Toulouse, Grenoble, France. [2]Institute of Physics, Chinese Academy of Sciences and Beijing National Laboratory for Condensed Matter Physics, Beijing, China. [3]National High Magnetic Field Laboratory, Florida State University, Tallahassee, FL, USA. [4]Université Grenoble Alpes, CNRS, Grenoble INP, Institut Néel, Grenoble, France. [5]Department of Physics, Hokkaido University, Sapporo, Japan. [6]Muroran Institute of Technology, Muroran, Japan. [7]Central Research Institute of Electric Power Industry, Yokosuka, Japan. [8]Department of Physics, University of Zurich, Zurich, Switzerland. [9]These authors contributed equally: Mehdi Frachet, Igor Vinograd.
✉e-mail: david.leboeuf@lncmi.cnrs.fr; marc-henri.julien@lncmi.cnrs.fr

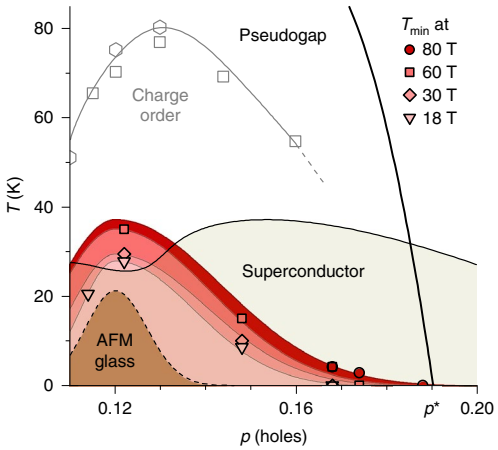


**Fig. 1 | Quasi-static magnetism in the pseudogap state of $La_{2-x}Sr_xCuO_4$.** Temperature–doping phase diagram representing $T_{min}$, the temperature at which the the sound velocity is minimum, at different fields. Because superconductivity precludes the observation of $T_{min}$ in zero field, the dashed line (brown area) represents the extrapolated $T_{min}(B=0)$. Although not exactly equal to the freezing temperature $T_f$ (see Fig. 2), $T_{min}$ is closely tied to $T_f$ and so is expected to have the same doping dependence, including a peak around $p=0.12$ in zero or low fields (ref. [3]). The thick black line that runs nearly vertically from $p^*=0.19$ at $T=0$ is the pseudogap temperature $T^*$. Onset temperatures of charge order are from ref. [32] (hexagons) and ref. [33] (squares). AFM glass, antiferromagnetic glass.

condition $\omega_{US}\tau_c=1$ corresponds to an inflexion point in $\Delta v/v(T)$ (see Extended Data Fig. 2). This is why $T_{min}$ is always slightly higher than $T_f$ defined from NMR (and this is not an effect of frequency, which is very similar for the two techniques). For $p=0.148$, the maximum in $1/T_1$ at $B=34$ T is found at $T_f=7\pm1$ K, whereas $T_{min}=10\pm2$ K (Fig. 2). Note that all ultrasound data presented here were obtained in the transverse acoustic mode $(c_{11}-c_{12})/2$. The spin-stripe pattern of $La_{2-x}Sr_xCuO_4$ inferred from neutron scattering data[16–18] is indeed prone to coupling with orthorhombic strains generated by this mode.

What we detect here is not a true phase transition as a function of temperature but an apparent freezing at the experimental (MHz) timescale: the moments continue to slow down (typically exponentially) on cooling below $T_f$ and become truly static at much lower temperatures, if not only at $T=0$. In principle, the temperature at which the staggered moments fluctuate more slowly than the $^{139}$La NMR linewidth of order 1 MHz can be detected as a line broadening[22]. However, this effect can be measured only for fields applied parallel to the ordered moments; that is, in the $CuO_2$ planes. Therefore, it is impossible to measure the ordered moment here as freezing occurs only for perpendicular fields (Fig. 2b and Extended Data Fig. 3).

We next investigated whether glassy freezing can be detected at higher doping. For doping levels $p=0.155$–$0.188$, data from both techniques are qualitatively similar to that for $p=0.148$ (Fig. 3g). A softening is observed in ultrasound upon cooling at low temperatures in high fields, although at lower temperatures than for $p=0.148$. In Fig. 3, we plot $1/T_1T$ instead of $1/T_1$ to better highlight the difference compared to the normal state at which $1/T_1T$ is constant just above $T_c$. Data for $1/T_1$ versus $T$ are displayed in Extended Data Fig. 5. Although a peak in $1/T_1$ versus $T$ is not observed for $p=0.171$ at our highest field, $1/T_1T$ values are much higher than expected from an extrapolation of the normal state values (Fig. 3c), thus showing that the effect of the field is not just to close the superconducting gap.

At base temperature ($T\sim1.5$ K), both $1/T_1$ and $(\Delta v/v)^{-1}$ grow with field strength (Fig. 4a,b) but the field scale required to observe this increase grows with doping (see also Extended Data Fig. 3). This is visualized in the doping dependence of the field scale $B_{slow}$ that characterizes the onset of slow spin fluctuations (Fig. 4c and Methods). Typically, $B_{slow}$ is the field above which an elastic response should appear in neutron scattering. At $p\approx0.17$, $B_{slow}\approx30$ T is already as high as roughly two-thirds of the upper critical field $B_{c2}$ (as defined from transport measurements, Supplementary Fig. 2). The existence of a doping-dependent field scale $B_{slow}$ (most clearly seen in the ultrasound data in Fig. 4b) suggests that the critical doping at which the antiferromagnetic glass appears at $T=0$ is shifted towards lower doping levels by superconductivity[26,27].

The above results are consistent with theories[26,27] in which spin order competes with superconductivity: the competing order is enhanced in and around vortex cores and progressively takes over superconductivity as the field, and thus the vortex density, increases. The absence of spin freezing when $B$ is parallel to the $CuO_2$ planes (Fig. 2b and Extended Data Fig. 3g) is consistent with the idea that magnetism is primarily induced by the weakening of superconductivity, not by the field itself.

There is, however, a fundamental aspect of the data that could not be anticipated by phenomenological theories of competing orders[26,27]: the competition is found to be a property of the pseudogap phase because field-dependent freezing ends at a doping $p\approx p^*$, as summarized in the phase diagram (Fig. 1). We draw this conclusion from the fact that the results for $p\approx0.21>p^*$ (Fig. 3 and Extended Data Figs. 3,8) are qualitatively different from those for $p<0.19$, without any evidence of field-dependent magnetism: the saturation of $1/T_1$ above 40 T $\approx B_{c2}$ at values close to those of the normal state shows that the modest field dependence is now entirely accounted for by the closure of the superconducting gap. Furthermore, extrapolation of $B_{slow}$ data to higher doping levels suggests that $B_{slow}$, if present, should be around 50 T for $p=0.215$. As this is well below the maximum field (85 T) achieved during the ultrasound experiments, any field-dependent magnetism in this sample should have been detected. This shows that the field scale $B_{slow}$ no longer exists at $p=0.215$ and no field-dependant spin freezing occurs at this doping level. Moreover, the absence of spin freezing for $p>p^*$ is also observed by ultrasound attenuation as shown in Extended Data Fig. 8: the attenuation at $p=0.215$ has a negligible field dependence, whereas an attenuation peak signalling magnetic freezing develops in high field for $p=0.168$.

Therefore, it appears that once superconductivity is quenched in high fields, the boundary of the pseudogap phase at $T=0$ is concomitant with a quantum phase transition from glassy antiferromagnetic order to a correlated metal with only short-lived antiferromagnetism. This is our main finding and below we explore its implications and possible interpretations.

An antiferromagnetic quantum critical point (meaning a second-order quantum phase transition) hidden by superconductivity has been observed previously in a heavy-fermion metal[28] and in an electron-doped cuprate[29]. Therefore, it would be tempting to infer that the cuprate pseudogap ends at such an antiferromagnetic quantum critical point. However, there are two reasons to not do so. First, we do not know whether the observed quantum phase transition at $p^*$ is first or second order: our experiments measure neither the spin-spin correlation length nor the ordered moment (see above), and they provide no evidence of a possible phase separation between magnetic and non-magnetic regions in each sample[30]. Second, the interpretations of refs. [28,29] (above) might also have been applied here if spin order appeared sharply at the pseudogap onset temperature $T^*$. However, this is not the case: spin fluctuations progressively slow down on cooling and freeze at temperatures that are one to two orders of magnitude lower than $T^*$. In La-based cuprates, spin and charge orders are generally intertwined[31], such that the freezing temperature of the spin glass, $T_g$, is enhanced by charge order around 1/8 doping[32,33]. Within this

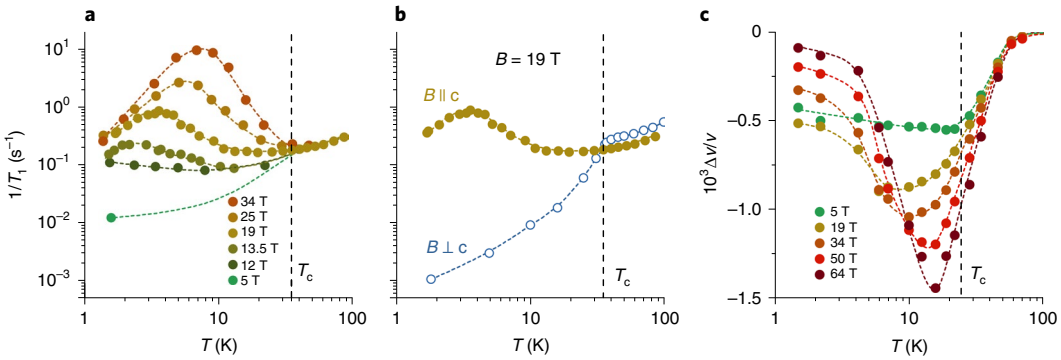


**Fig. 2 | NMR and ultrasound signatures of field-dependent glassy freezing in $La_{1.852}Sr_{0.148}CuO_4$. a**, $^{139}$La $1/T_1$ versus temperature at different fields (applied parallel to the crystallographic *c* axis). The broad peak in $1/T_1$ is characteristic of the continuous slowing down of spin fluctuations, with a correlation time diverging towards $T \approx 0$ (typically $\tau_c = \tau_\infty \exp(E_0/k_B T)$ with an activation energy $E_0$). The peak amplitude decreases and its width increases with decreasing *B* such that the peak is no longer discerned at low fields. We notice that $1/T_1$ varies with field strength between 25 and 34 T at $T > 10$ K where the sample should be in the normal state (at finite temperatures and fields, $T_c$ is no longer a true phase transition and thus it is experimentally ill-defined). This field dependence may arise from several effects or from a combination thereof: first, spin freezing may compete with superconducting fluctuations, thus leading to a field dependence above $T_c$ and/or above the resistive $B_{c2}$ and, second, there is probably a distribution of $B_{c2}$ values originating from doping inhomogeneity[46] and/or from indirect effects of disorder[47,48]. **b**, $^{139}$La $1/T_1$ versus temperature at $B = 19$ T applied parallel or perpendicular to the *c* axis. For $B \perp c$, $1/T_1$ drops strongly below $T_c$, as expected for a superconductor, without any sign of enhanced spin fluctuations. **c**, Sound velocity $\Delta v/v$ in the $(c_{11} - c_{12})/2$ mode versus temperature at different fields (applied parallel to the *c* axis), after subtraction of a lattice background (see Methods). In spin glasses, the softening (decrease of $\Delta v/v$ upon cooling) mirrors the increase of a susceptibility above the freezing temperature $T_f$ (ref. [25]). There is a minimum in $\Delta v/v$ at $T_{min}$ before the lattice hardens upon further cooling through $T_f$ (see text and Extended Data Fig. 2). Such a dip in $\Delta v/v$ has been reported earlier in $La_{1.86}Sr_{0.14}CuO_4$ at lower fields[49] and was interpreted as the result of a competition between a structural instability (producing a softening above $T_c$) and superconductivity (producing a hardening below $T_c$). Our measurements up to 64 T show that the minimum in $\Delta v/v$ cannot be due to superconductivity as it gets deeper and is shifted to higher temperatures as the field increases. Dashed lines connecting the data points are guides to the eye.

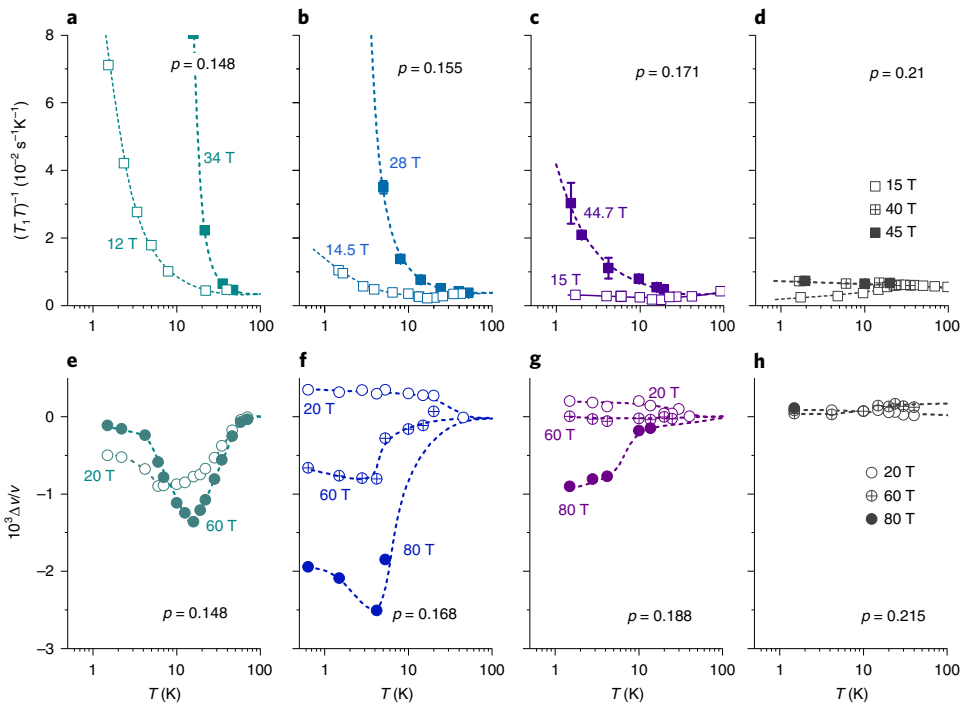


**Fig. 3 | Doping dependence of spin freezing in high fields. a–d**, $^{139}$La $1/T_1T$ versus temperature at different fields and hole doping levels. For $p = 0.21$, $1/T_1$ saturates in high fields at values extrapolated from $T > T_c$, meaning that the field effect on $1/T_1$ arises from the closure of the superconducting gap. Notice that $1/T_1$ values for this compound are extrinsically high owing to lattice fluctuations at low temperature (Extended Data Fig. 4). **e–h**, Sound velocity $\Delta v/v$ versus temperature at different fields and hole doping levels. For $p = 0.168$ and 0.188, $\Delta v/v$ at $B = 20$ T increases upon cooling and saturates at low temperature. This behaviour is explained by the coupling of superconductivity with the lattice (see Methods). With increasing *B*, this superconducting contribution to the sound velocity is reduced and a lattice softening develops. For $p = 0.215$, $\Delta v/v$ shows almost no temperature dependence up to 80 T and down to 1.5 K. Notice that, although we detect slow spin fluctuations up to $p = 0.188$, freezing at the NMR or ultrasound timescales (both in the MHz range) is not reached in two of our datasets: for $p = 0.171$, $1/T_1T$ is anomalously enhanced in high fields (**c** and Fig. 4a), but there is no peak of $1/T_1$ versus *T* even at 45 T (Extended Data Fig. 5). For $p = 0.188$, we observe a lattice softening but not the hardening that signals the frozen state, at least down to 1.5 K in a field of 80 T. Dashed lines are guides to the eye.

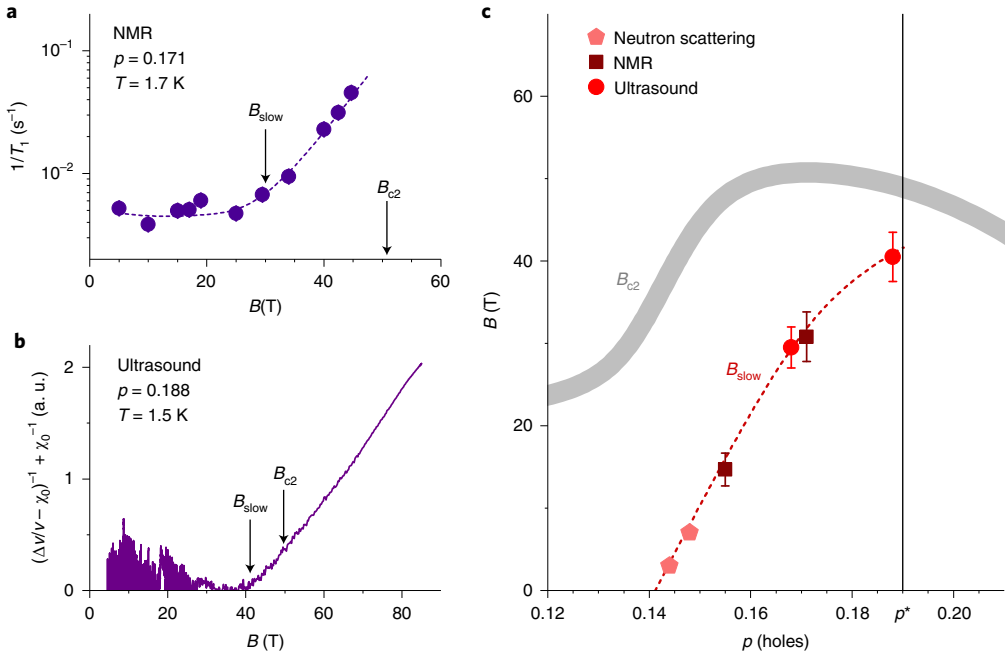


**Fig. 4 | Field dependence of quasi-static magnetism. a**, Field dependence of $^{139}$La $1/T_1$ at $T=1.7$ K for $p=0.171$ (see Extended Data Fig. 3 for additional doping levels). The arrow points to the onset field of slow spin fluctuations $B_{slow}$ (defined so as to match the neutron onset field for $p=0.148$ (ref. [18]), as explained in the Methods section). **b**, Field dependence of $(\Delta v/v - \chi_0)^{-1} + \chi_0^{-1}$ (in arbitrary units (a. u.)) for $p=0.188$ and $T=1.5$ K ($\geq T_{min}$), where $\chi_0$ is a doping-dependent constant (see Extended Data Fig. 3 for additional doping levels). $\Delta v/v$ is almost field independent at low fields, but above a doping-dependent onset field $B_{slow}$ (indicated by an arrow), it shows a clear $1/B$ dependence. Note that, within error bars, $B_{slow}$ has no temperature dependence between 0.6 K and 4.2 K, for $p=0.168$ (Extended Data Fig. 6). **c**, Doping dependence of $B_{slow}$ and $B_{c2}$ (see Supplementary Fig. 2). Error bars on the value of $B_{slow}$ inferred from ultrasound measurements are estimated from the uncertainty on the field above which $(\Delta v/v - \chi_0)^{-1}$ deviates from linearity. Error bars for the values of $B_{slow}$ from NMR are estimated from the uncertainty in the determination procedure shown in Extended Data Fig. 7. Dashed lines are guides to the eye.

perspective, the disappearance of the spin glass near $p^\star$ prompts an investigation of whether the fates of spin and charge orders are still connected near $p^\star$ or whether these two phenomena become disconnected.

Together with previous reports of spin glass at lower doping[3,4], our work shows that the spin glass spans from the weakly doped insulator at $p=0.02$ all the way up to $p^\star \approx 0.19$. This suggests that the same local-moment antiferromagnetism as that found in the doped Mott insulator[34] survives throughout the pseudogap state. This observation favours scenarios in which the pseudogap state originates from strong correlation physics rooted in the doped Mott insulator (for example, ref. [35]).

Our results are relevant to the interpretation of high-field experiments performed in La-based cuprates. Indeed, central to the interpretation of these experiments is the idea that the properties of the field-induced normal state may serve as a proxy for the whole pseudogap state; that is, at temperatures up to $T^\star$. Our results suggest that this is not necessarily so: in $La_{2-x}Sr_xCuO_4$, the field-induced normal state at $T=0$ is an ordered antiferromagnet (albeit freezing like a glass), but the temperature-induced normal state ($T > T_c$) shows only short-lived antiferromagnetic correlations.

This distinction should hold for transport[36–40] properties, as these are known to be influenced by magnetic correlations. If correlated over sufficiently long distances (the correlation length $\xi_{AF} > 100$ lattice spacings in $La_{1.88}Sr_{0.12}CuO_4$ (ref. [16])), the frozen striped antiferromagnetic pattern should affect low-lying electronic states[41] and thus, as noted in refs. [40,42], affect transport measurements at low temperatures and high fields, up to $p^\star$. As a matter of fact, the possible relationship between spin-glass freezing and resistivity upturns has long been discussed in the literature (see, for example, refs. [5,42,43] and references therein).

Recent specific-heat measurements of $La_{1.6-x}Nd_{0.4}Sr_xCuO_4$ in high fields have led to the conclusion that the pseudogap ends at a quantum critical point[44]. This raises the question of whether the pseudogap phase is an ordered state at all temperatures up to $T^\star$ (see refs. [1,2,31] and references therein). The fact that $La_{1.6-x}Nd_{0.4}Sr_xCuO_4$ probably shows a similar field dependence for spin and charge correlations as in $La_{2-x}Sr_xCuO_4$ (ref. [45]) suggests that the observed quantum criticality in $La_{1.6-x}Nd_{0.4}Sr_xCuO_4$ might arise, not from the pseudogap phase itself, but from a consequence of it in this material: a magnetic quantum phase transition occurring at $p^\star$. This possibility indicates that the observation of quantum criticality in high fields does not necessarily mean that the pseudogap is an ordered state. Further insight into this issue might come from neutron scattering experiments in high fields to determine whether the magnetic quantum phase transition is first or second order.

## Online content

Any methods, additional references, Nature Research reporting summaries, source data, extended data, supplementary information, acknowledgements, peer review information; details of author contributions and competing interests; and statements of data and code availability are available at https://doi.org/10.1038/s41567-020-0950-5.

Received: 4 October 2019; Accepted: 28 May 2020;
Published online: 06 July 2020

## References

1. Keimer, B., Kivelson, S. A., Norman, M. R., Uchida, S. & Zaanen, J. From quantum matter to high-temperature superconductivity in copper oxides. *Nature* **518**, 179–186 (2015).

2. Proust, C. & Taillefer, L. The remarkable underlying ground states of cuprate superconductors. *Annu. Rev. Condens. Matter Phys.* **10**, 409–429 (2019).
3. Julien, M.-H. Magnetic order and superconductivity in $La_{2-x}Sr_xCuO_4$: a review. *Phys. B* **329**, 693 (2003).
4. Niedermayer, C. H. et al. Common phase diagram for antiferromagnetism in $La_{2-x}Sr_xCuO_4$ and $Y_{1-x}Ca_xBa_2Cu_3O_6$ as seen by muon spin rotation. *Phys. Rev. Lett.* **80**, 3843–3846 (1998).
5. Julien, M.-H. et al. Charge segregation, cluster spin glass, and superconductivity in $La_{1.94}Sr_{0.06}CuO_4$. *Phys. Rev. Lett.* **83**, 604–607 (1999).
6. Panagopoulos, C. et al. Low-frequency spins and the ground state in high-$T_c$ cuprates. *Solid State Commun.* **126**, 47–55 (2003).
7. Risdiana et al. Cu spin dynamics in the overdoped regime of $La_{2-x}Sr_xCu_{1-y}Zn_yO_4$ probed by muon spin rotation. *Phys. Rev. B.* **77**, 054516 (2008).
8. Haug, D. et al. Neutron scattering study of the magnetic phase diagram of underdoped $YBa_2Cu_3O_{6+x}$. *New J. Phys.* **12**, 105006 (2010).
9. Wu, T. et al. Magnetic-field-enhanced spin freezing on the verge of charge ordering in $YBa_2Cu_3O_{6.45}$. *Phys. Rev. B* **88**, 014511 (2013).
10. Sasagawa, T., Mang, P. K., Vajk, O. P., Kapitulnik, A. & Greven, M. Bulk magnetic properties and phase diagram of Li-doped $La_2CuO_4$: Common magnetic response of hole-doped $CuO_2$ planes. *Phys. Rev. B* **66**, 184512 (2002).
11. Kimura, H. et al. Novel in-gap spin state in Zn-doped $La_{1.85}Sr_{0.15}CuO_4$. *Phys. Rev. Lett.* **91**, 067002 (2003).
12. Tallon, J. L., Loram, J. W. & Panagopoulos, C. Pseudogap and quantum-transition phenomenology in HTS cuprates. *J. Low Temp. Phys.* **131**, 387–394 (2003).
13. Julien, M.-H. et al. $^{63}$Cu NMR evidence for enhanced antiferromagnetic correlations around Zn impurities in $YBa_2Cu_3O_{6.7}$. *Phys. Rev. Lett.* **84**, 3422–3425 (2000).
14. Alloul, H., Bobroff, J., Gabay, M. & Hirschfeld, P. J. Defects in correlated metals and superconductors. *Rev. Mod. Phys.* **81**, 45–108 (2009).
15. Li, Y. et al. Low-energy antiferromagnetic spin fluctuations limit the coherent superconducting gap in cuprates. *Phys. Rev. B* **98**, 224508 (2018).
16. Lake, B. et al. Antiferromagnetic order induced by an applied magnetic field in a high-temperature superconductor. *Nature* **415**, 299–302 (2002).
17. Khaykovich, B. et al. Field-induced transition between magnetically disordered and ordered phases in underdoped $La_{2-x}Sr_xCuO_4$. *Phys. Rev. B* **71**, 220508 (2005).
18. Chang, J. et al. Tuning competing orders in $La_{2-x}Sr_xCuO_4$ cuprate superconductors by the application of an external magnetic field. *Phys. Rev. B* **78**, 104525 (2008).
19. Lake, B. et al. Spins in the vortices of a high-temperature superconductor. *Science* **291**, 1759–1762 (2001).
20. Tranquada, J. M. et al. Evidence for an incommensurate magnetic resonance in $La_{2-x}Sr_xCuO_4$. *Phys. Rev. B* **69**, 174507 (2004).
21. Mitrović, V. F. et al. Similar glassy features in the $^{139}$La NMR response of pure and disordered $La_{1.88}Sr_{0.12}CuO_4$. *Phys. Rev. B* **78**, 014504 (2008).
22. Arsenault, A. et al. $^{139}$La NMR investigation of the charge and spin order in a $La_{1.885}Sr_{0.115}CuO_4$ single crystal. *Phys. Rev. B* **97**, 064511 (2018).
23. Baek, S.-H., Erb, A. & Büchner, B. Low-energy spin dynamics and critical hole concentrations in $La_{2-x}Sr_xCuO_4$ ($0.07 \leq x \leq 0.2$) revealed by $^{139}$La and $^{63}$Cu nuclear magnetic resonance. *Phys. Rev. B* **96**, 094519 (2017).
24. Curro, N. J. et al. Inhomogeneous low frequency spin dynamics in $La_{1.65}Eu_{0.2}Sr_{0.15}CuO_4$. *Phys. Rev. Lett.* **85**, 642 (2000).
25. Doussineau, P., Levelut, A., Matecki, M., Renard, J. P. & Schön, W. Acoustic and magnetic studies of an insulating spin glass. *EPL* **3**, 251 (1987).
26. Demler, E., Sachdev, S. & Zhang, Y. Spin-ordering quantum transitions of superconductors in a magnetic field. *Phys. Rev. Lett.* **87**, 067202 (2001).
27. Kivelson, S. A., Lee, D.-H., Fradkin, E. & Oganesyan, V. Competing order in the mixed state of high-temperature superconductors. *Phys. Rev. B* **66**, 144516 (2002).
28. Park, T. et al. Hidden magnetism and quantum criticality in the heavy fermion superconductor $CeRhIn_5$. *Nature* **440**, 65–68 (2006).
29. Kang, H. J. et al. Antiferromagnetic order as the competing ground state in electron-doped $Nd_{1.85}Ce_{0.15}CuO_4$. *Nature* **423**, 522–525 (2003).
30. Wakimoto, S. et al. Disappearance of antiferromagnetic spin excitations in overdoped $La_{2-x}Sr_xCuO_4$. *Phys. Rev. Lett.* **98**, 247003 (2007).
31. Fradkin, E., Kivelson, S. A. & Tranquada, J. M. Theory of intertwined orders in high temperature superconductors. *Rev. Mod. Phys.* **87**, 457–482 (2015).
32. Croft, T. P., Lester, C., Senn, M. S., Bombardi, A. & Hayden, S. M. Charge density wave fluctuations in $La_{2-x}Sr_xCuO_4$ and their competition with superconductivity. *Phys. Rev. B* **89**, 224513 (2014).
33. Wen, J. J. et al. Observation of two types of charge density wave orders in superconducting $La_{2-x}Sr_xCuO_4$. *Nat. Commun.* **10**, 3269 (2019).
34. Parcollet, O. & Georges, A. Non-Fermi-liquid regime of a doped Mott insulator. *Phys. Rev. B* **59**, 5341–5360 (1999).
35. Sordi, G., Haule, K. & Tremblay, A.-M. S. Finite Doping Signatures of the Mott Transition in the Two-Dimensional Hubbard Model. *Phys. Rev. Lett.* **104**, 226402 (2010).
36. Boebinger, G. S. et al. Insulator-to-metal crossover in the normal state of $La_{2-x}Sr_xCuO_4$ near optimum doping. *Phys. Rev. Lett.* **77**, 5417–5420 (1996).
37. Balakirev, F. F. et al. Quantum phase transition in the magnetic-field-induced normal state of optimum-doped high-$T_c$ cuprate superconductors at low temperatures. *Phys. Rev. Lett.* **102**, 017004 (2009).
38. Cooper, R. A. et al. Anomalous criticality in the electrical resistivity of $La_{2-x}Sr_xCuO_4$. *Science* **323**, 603–607 (2009).
39. Collignon, C. et al. Fermi-surface transformation across the pseudogap critical point of the cuprate superconductor $La_{1.6-x}Nd_{0.4}Sr_xCuO_4$. *Phys. Rev. B* **95**, 224517 (2017).
40. Bourgeois-Hope, P. et al. Link between magnetism and resistivity upturn in cuprates: a thermal conductivity study of $La_{2-x}Sr_xCuO_4$. Preprint at https://arxiv.org/abs/1910.08126 (2019).
41. Millis, A. J. & Norman, M. R. Antiphase stripe order as the origin of electron pockets observed in 1/8-hole-doped cuprates. *Phys. Rev. B* **76**, 220503 (2007).
42. Sun, X. F., Komiya, S., Takeya, J. & Ando, Y. Magnetic-field-induced localization of quasiparticles in underdoped $La_{2-x}Sr_xCuO_4$ single crystals. *Phys. Rev. Lett.* **90**, 117004 (2003).
43. Panagopoulos, C. & Dobrosavljević, V. Self-generated electronic heterogeneity and quantum glassiness in the high-temperature superconductors. *Phys. Rev. B* **72**, 014536 (2005).
44. Michon, B. et al. Thermodynamic signatures of quantum criticality in cuprate superconductors. *Nature* **567**, 218–222 (2019).
45. Hücker, M. et al. Enhanced charge stripe order of superconducting $La_{2-x}Ba_xCuO_4$ in a magnetic field. *Phys. Rev. B* **87**, 014501 (2013).
46. Singer, P. M., Hunt, W. A. & Imai, T. $^{63}$Cu NQR evidence for spatial variation of hole concentration in $La_{2-x}Sr_xCuO_4$. *Phys. Rev. Lett.* **88**, 047602 (2002).
47. Yu, Y. & Kivelson, S. A. Fragile superconductivity in the presence of weakly disordered charge density waves. *Phys. Rev. B* **99**, 144513 (2019).
48. Leridon, B. et al. Protected superconductivity at the boundaries of charge-density-wave domains. Preprint at https://arxiv.org/abs/1905.05606 (2019).
49. Nohara, M. et al. Interplay between lattice softening and high-$T_c$ superconductivity in $La_{1.86}Sr_{0.14}CuO_4$. *Phys. Rev. Lett.* **70**, 3447 (1993).

## Methods

**Samples.** High-quality $La_{2-x}Sr_xCuO_4$ single crystals were grown by the travelling solvent floating zone method. NMR samples with $x=p=0.171$ and $x=p=0.210$ were cut from the same rods as the ultrasound samples with $p=0.168$ and $p=0.215$, respectively (see below for the estimation of $p$ values).

**Determination of doping level.** The hole doping $p$, which is considered to be equal to the Sr concentration $x$ in the absence of oxygen off-stoichiometry, has been determined by measuring $T_{st}$, the temperature of the structural transition from the high-$T$ tetragonal (HTT) phase to the low-$T$ orthorhombic (LTO) phase[50,51], either by NMR or by sound velocity (Extended Data Fig. 9). $T_{st}$ provides a more accurate measurement of doping than $T_c$ because it varies more strongly with hole doping and is less sensitive to defects. In NMR samples, $T_{st}$ was measured using the spin-lattice relaxation rate $1/T_1$ of $^{139}$La, which shows a peak at the transition (Extended Data Fig. 4 and refs. [22,23]). In ultrasound samples it was detected by measuring the $(c_{11}-c_{12})/2$ mode, which shows an anomaly at the transition (Extended Data Fig. 10).

Given that the HTT to LTO transition line decreases to 0 at $p\approx0.21$, the doping of samples with Sr content above this value is assessed using the superconducting critical temperature $T_c$. $T_c$ of NMR samples was measured by tracking the resonance frequency of the NMR tank circuit, which showed a strong and very sharp change at $T_c$ for all samples. In ultrasound samples, an anomaly at $T_c$ is detected in the temperature dependence of the sound velocity $\Delta v/v$ (see Supplementary Fig. 1).

Supplementary Table 1 summarizes the properties of the single crystals used in this study. The typical (relative) uncertainty on doping is $\pm0.002$ hole per Cu site, except for $p\geq0.21$ for which it is $\pm0.005$ hole per Cu site.

**Ultrasound measurements.** Transverse ultrasonic waves at typical frequencies ranging from 150 MHz to 250 MHz (see Extended Data Fig. 6 for measurement frequencies at each doping level) were generated using commercial $LiNbO_3$ 41° X-cut transducers (Boston Piezo-Optics) glued on oriented, polished and cleaned surfaces. We used a special set-up to orient the crystal in a Laue diffractometer and to transfer the crystal on a wire saw while conserving its orientation within a typical precision of one degree.

A standard pulse-echo technique with phase comparison was used to measure sound velocity variation $\Delta v/v$ (ref. [52]). The experiments were performed at the LNCMI Toulouse in pulsed fields with strengths of up to 86 T. A high-speed acquisition system was used to record the evolution of the phase of the acoustic echoes during the magnetic field pulse. When possible, we checked for reproducibility at different frequencies and on different echoes. Data on the upsweep and downsweep of the magnetic field pulses showed good overlap, indicating that the temperature of the sample was constant during the pulse. The field dependence of the sound velocity at different temperatures is shown for all samples in Extended Data Fig. 6.

**Contributions to the sound velocity.** The measurements in pulsed fields allow for the determination of the field-induced sound velocity, $\Delta v/v(B)$, at different temperatures (Extended Data Fig. 6). By performing constant-field cuts in these field sweeps, we obtain the temperature dependence of the field-dependent sound velocity. To obtain the complete temperature dependence of the sound velocity $\Delta v/v$ at different fields (Figs. 2,3), we need to add the zero-field electronic sound velocity, $\Delta v/v(B=0)_e$:

$$\Delta v/v = \Delta v/v(B) + \Delta v/v(B=0)_e \tag{1}$$

The term $\Delta v/v(B=0)_e$ includes the influence of superconductivity and magnetism on the lattice. It is extracted from the raw data of the zero-field temperature-dependent sound velocity, $\Delta v/v(B=0)$, which also contains a background component, $\Delta v/v(B=0)_{background}$. This background term originates from the natural hardening of the lattice as the sample is cooled. This background is fitted, within a temperature range in which neither magnetism nor superconductivity makes a significant contribution to $\Delta v/v(B=0)$, with an empirical formula:

$$\Delta v/v(B=0)_{background} = c - \frac{s}{\exp\left(\frac{t}{T}\right)-1} \tag{2}$$

Equation (2) has been shown to describe accurately the lattice contribution to the elastic constant in a wide variety of systems[53], including cuprates[54]. Supplementary Fig. 1 shows the zero-field sound velocity data $\Delta v/v(B=0)$, the background fit $\Delta v/v(B=0)_{background}$ and the extracted zero-field electronic contribution $\Delta v/v(B=0)_e$.

**NMR measurements.** Experiments were performed using standard spin-echo techniques and home-built heterodyne spectrometers in direct current fields provided by superconducting and resistive magnets at the LNCMI, Grenoble, France, and the hybrid magnet at the NHMFL, Tallahassee, USA.

The spin-lattice relaxation time $T_1$ was determined by fitting the saturation-recovery curve of the $^{139}$La magnetization to a stretched multi-exponential given by equation (3), which is valid for the purely magnetic relaxation of the central line of a nuclear spin 7/2. The stretching exponent $\beta$ accounts phenomenologically for the distribution of $T_1$ values (ref. [21] and references therein) that develops at low temperatures and makes $\beta$ deviate from 1 (Extended Data Fig. 1). Then, $T_1$ corresponds to the median relaxation rate.

$$\begin{aligned}\frac{^{139}M_0 - {}^{139}M_z(t)}{^{139}M_0} &= \frac{1225}{1716}\exp\left[-\left(\frac{28t}{T_1}\right)^{\beta}\right] + \frac{75}{364}\exp\left[-\left(\frac{15t}{T_1}\right)^{\beta}\right] \\ &+ \frac{3}{44}\exp\left[-\left(\frac{6t}{T_1}\right)^{\beta}\right] + \frac{1}{84}\exp\left[-\left(\frac{t}{T_1}\right)^{\beta}\right]\end{aligned} \tag{3}$$

The same expression was used for all temperatures despite the presence of quadrupole relaxation (which is produced by electric-field gradient fluctuations and described by a different form of recovery) around the structural transition temperature, which causes the exponent $\beta$ to deviate from 1.

**NMR determination of the field scale $B_{slow}$.** The only prominent feature seen in the NMR data is the temperature $T_f$ of the peak in $1/T_1$ versus $T$ (Fig. 2a). However, it is impossible to define a field strength above which this peak is present and it is also impossible to determine whether such a field actually exists. This is because when the field decreases, the peak intensity decreases and its width increases, which makes the peak gradually less well defined at low fields (Fig. 2a). We also cannot use an arbitrary criterion for the freezing because this would require extrapolation of the data for the $p=0.171$ sample. The range of fields (up to 45 T) and temperatures (down to 1.7 K) explored here do not reach the regime in which the peak in $1/T_1$ versus $T$ is found for this level of doping. Given that it is impossible to define the field above which spins are frozen at the NMR timescale, we determine the onset field of slow fluctuations. As there is no clear spike in the field dependence of $1/T_1$, we define $B_{slow}$ as the field at which the value of $1/T_1$ of a given sample is equal to the value of $1/T_1$ in the $p=0.148$ sample at $B=7$ T, which is the threshold field at which neutron scattering experiments detect a quasi-elastic response[18]. So, by definition, $B_{slow}=7$ T for $p=0.148$. Given that the criterion is chosen so that NMR and neutron scattering onset fields match at $p=0.148$, there is no NMR point for this sample in Fig. 4c. It turns out that the so-defined $B_{slow}$ in NMR matches the $B_{slow}$ defined from ultrasound (Fig. 4c).

However, for the determination of $B_{slow}$, we do not use directly the 'bare' experimental $T_1$ values because these are (slightly) biased by two effects. First, part of the field dependence is due to the reduction of the superconducting gap. Second, $1/T_1$ has an intrinsic $1/B$ dependence (see low-field upturns in Extended Data Fig. 7a), which indicates that, although $1/T_1$ has not yet reached its peak at $B_{slow}$, we are already sufficiently close to the resonance condition ($\omega\tau_c=1$) that $1/T_1 \propto 1/\omega \propto 1/B$, as expected for a mechanism of similar type to a Bloembergen–Purcell–Pound mechanism.

Therefore, for the sole purpose of determining $B_{slow}$ from NMR, we use $T_1$ data corrected by a factor of $1/B$ and from which an approximate field-dependent superconducting component has been subtracted (the evaluation of this background is detailed in Supplementary Fig. 3 and Extended Data Fig. 7).

We emphasize that these corrections are small (see Supplementary Fig. 3 and Extended Data Fig. 7) and that they do not affect the conclusions of this paper.

## Data availability

Data are available from the corresponding authors upon request.

## References


50. Wakimoto, S. et al. Incommensurate lattice distortion in the high temperature tetragonal phase of $La_{2-x}(Sr,Ba)_xCuO_4$. *J. Phys. Soc. Jpn.* **75**, 074714 (2006).
51. Takagi, H. et al. Disappearance of superconductivity in overdoped $La_{2-x}Sr_xCuO_4$ at a structural phase boundary. *Phys. Rev. Lett.* **68**, 3777–3780 (1992).
52. Lüthi, B. *Physical acoustics in the solid state* 1st edn, (Springer-Verlag, 2005).
53. Varshni, P. Temperature dependence of the elastic constants. *Phys. Rev. B* **2**, 3952–3958 (1970).
54. Nohara, M. et al. Unconventional lattice stiffening in superconducting $La_{2-x}Sr_xCuO_4$ single crystals. *Phys. Rev. B* **52**, 570–580 (1995).


## Acknowledgements


We thank G. S. Boebinger, A. Böhmer, N. B. Christensen, Y. Gallais, A. Georges, M. Greven, Z. Guguchia, S. M. Hayden, M. Horvatić, S. A. Kivelson, T. Klein, N. Laflorencie, M. Le Tacon, W. Metzner, C. Pépin, D. Popović, B. Ramshaw, A. T. Rømer, J. Schmalian, L. Taillefer, J. M. Tranquada and A. -M. Tremblay for discussions. Part of this work was performed at the LNCMI, a member of the European Magnetic Field Laboratory. A portion of this work was performed at the National High Magnetic Field Laboratory, which is supported by the US National Science Foundation Cooperative Agreement no. DMR-1644779 and the State of Florida. Work in Grenoble was supported by the Laboratoire d'Excellence LANEF (ANR-10-LABX-51-01). Work in Toulouse was supported through the EUR grant NanoX no. ANR-17-EURE-0009. Work at the LNCMI was supported by the French Agence Nationale de la Recherche (ANR) under reference ANR-19-CE30-0019 (Neptun). Work in Beijing was supported by the National Natural

Science Foundation of China (grant nos. 11674377, 11634015 and 11974405), MOST grants (no. 2016YFA0300502 and no. 2017YFA0302904) and the Strategic Priority Research Program of the Chinese Academy of Sciences (grant no. XDB33010100). Work in Zürich was supported by the Swiss National Science Foundation. S.O. acknowledges support from JSPS KAKENHI grant no. JP17H01052.

## Author contributions

M.F., S.B., S.W., C.P. and D.L. performed the ultrasound experiments. I.V., R.Z., H.M., S.K., S.K.R., A.P.R. and M.-H.J. performed the NMR experiments. M.F. and I.V. analysed experimental data with suggestions from D.L. and M.-H.J. T.K., N.M., M.O., S.K., S.O., M.H. and J.C. provided single crystals. M.F. and J.D. cut precisely oriented single crystals. D.L. and M.-H.J. supervised the project and wrote the manuscript with suggestions from all authors.

## Competing interests

The authors declare no competing interests.

## Additional information

**Extended data** is available for this paper at https://doi.org/10.1038/s41567-020-0950-5.

**Supplementary information** is available for this paper at https://doi.org/10.1038/s41567-020-0950-5.

**Correspondence and requests for materials** should be addressed to D.L. or M.-H.J.

**Peer review information** *Nature Physics* thanks Yuji Furukawa, Subir Sachdev and the other, anonymous, reviewer(s) for their contribution to the peer review of this work.

**Reprints and permissions information** is available at www.nature.com/reprints.

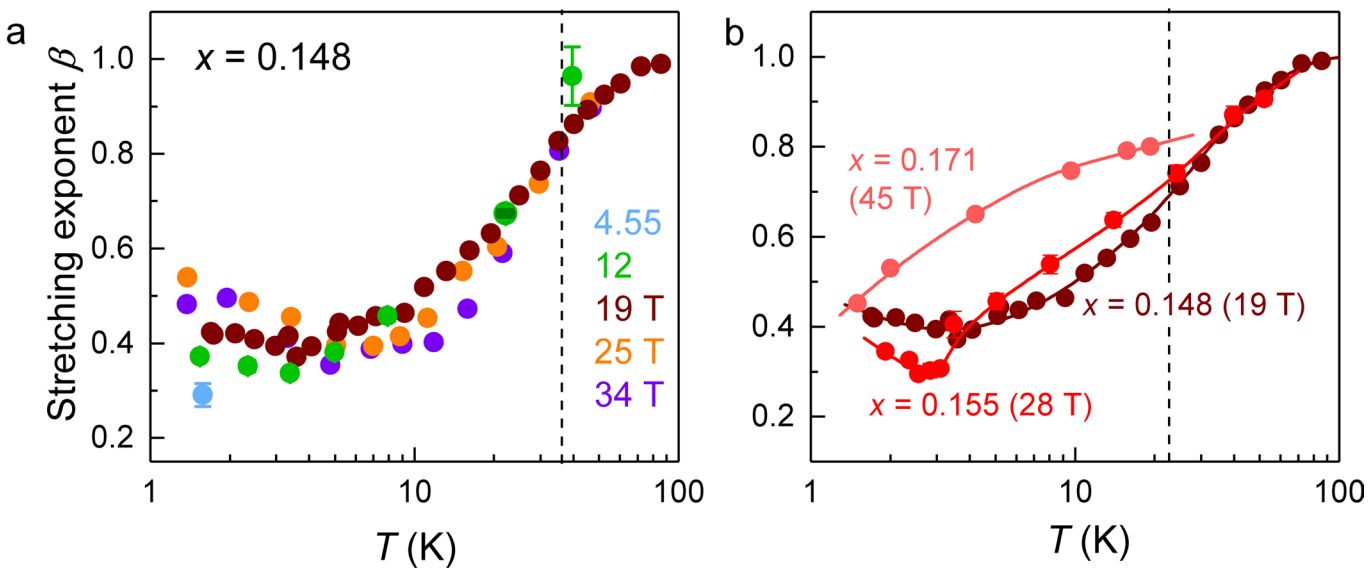


**Extended Data Fig. 1 | Stretching exponent $\beta$ in NMR $T_1$ measurements. a**, Stretching exponent $\beta$ for different fields in $La_{1.852}Sr_{0.148}CuO_4$. **b**, Stretching exponent $\beta$ for Sr concentrations $x = p$. The stretching exponent provides a phenomenological measure of the width of the distribution of $T_1$ values (ref.[21] and references therein).

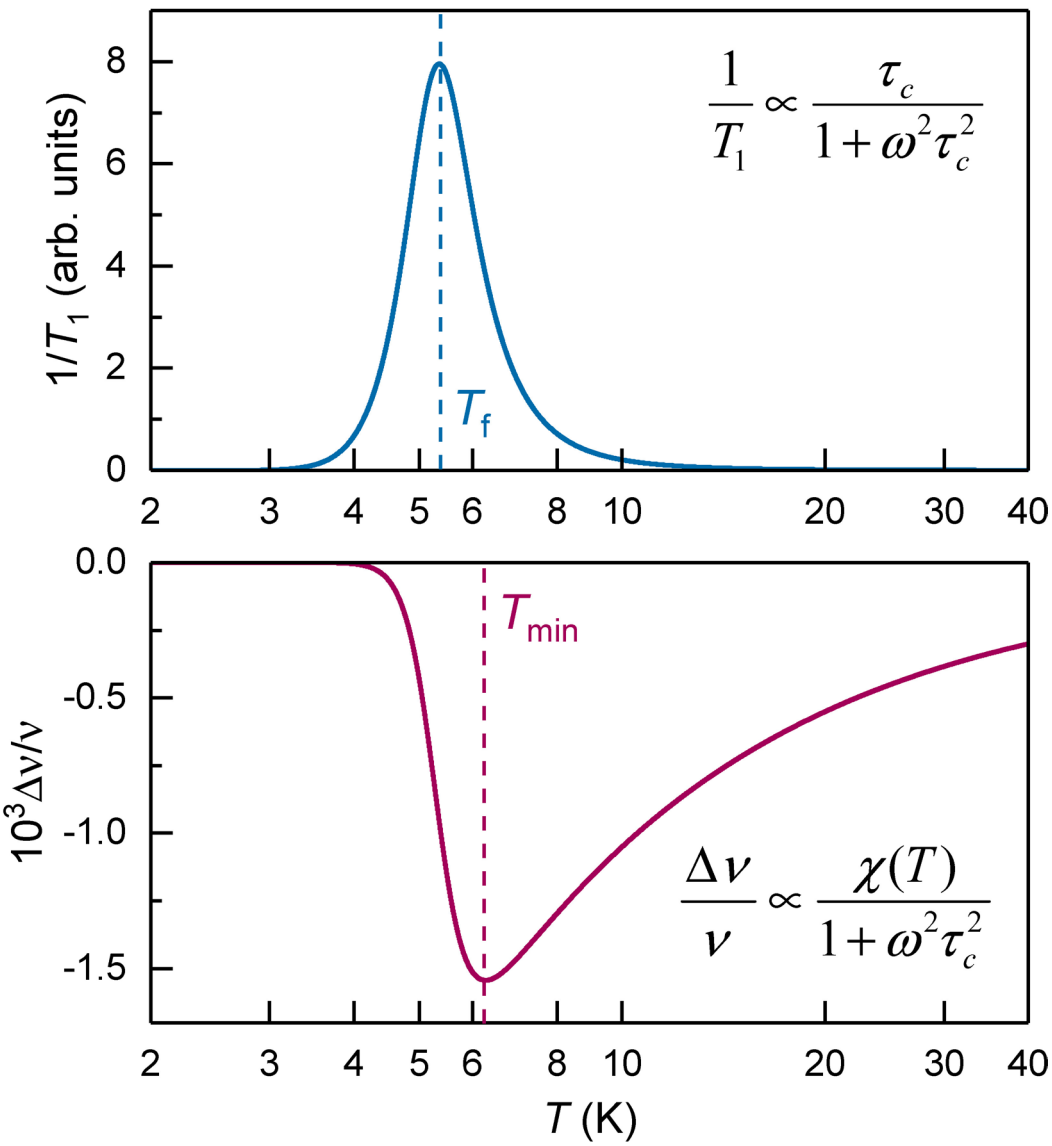


**Extended Data Fig. 2 | Comparison of $T_f$ from NMR and $T_{min}$ from sound velocity.** In the upper panel we show the temperature dependence of $1/T_1$ calculated within the BPP model with a correlation time $\tau_c \propto exp(1/T)$. Within this model, $1/T_1$ features a maximum when $\omega\,\tau_c = 1$. This maximum occurs at $T = T_f$ the freezing temperature at the NMR time scale. In the lower panel we plot the temperature dependence of the sound velocity $\Delta v/v$ calculated within the dynamical susceptibility model that applies to canonical spin glass systems[25]. We use the same correlation time $\tau_c$ as for $1/T_1$ calculation and we use a Curie-like susceptibility (T) $\propto$ 1/T. In contrast with $1/T_1$, the condition $\omega\,\tau_c = 1$ results in an inflexion point in $\Delta v/v$. The sound velocity minimum at $T_{min}$ is found slightly higher than $T_f$, as observed experimentally. The temperature dependence of the sound velocity can be understood as follows. At high temperature, when the ultrasound frequency $\omega_{US}$ is such that $\omega_{US} << \tau_c^{-1}$, a softening arises from the slowing down of acoustic phonons by magnetic fluctuations, through magneto-elastic coupling. On the other hand, in the frozen state at low temperature, when $\omega_{US} >> \tau_c^{-1}$, the acoustic phonons decouple from the slowly fluctuating moments leading to the hardening upon cooling. In between these two asymptotic behaviours, $\Delta v/v$ must go through a minimum at a temperature $T_{min}$.

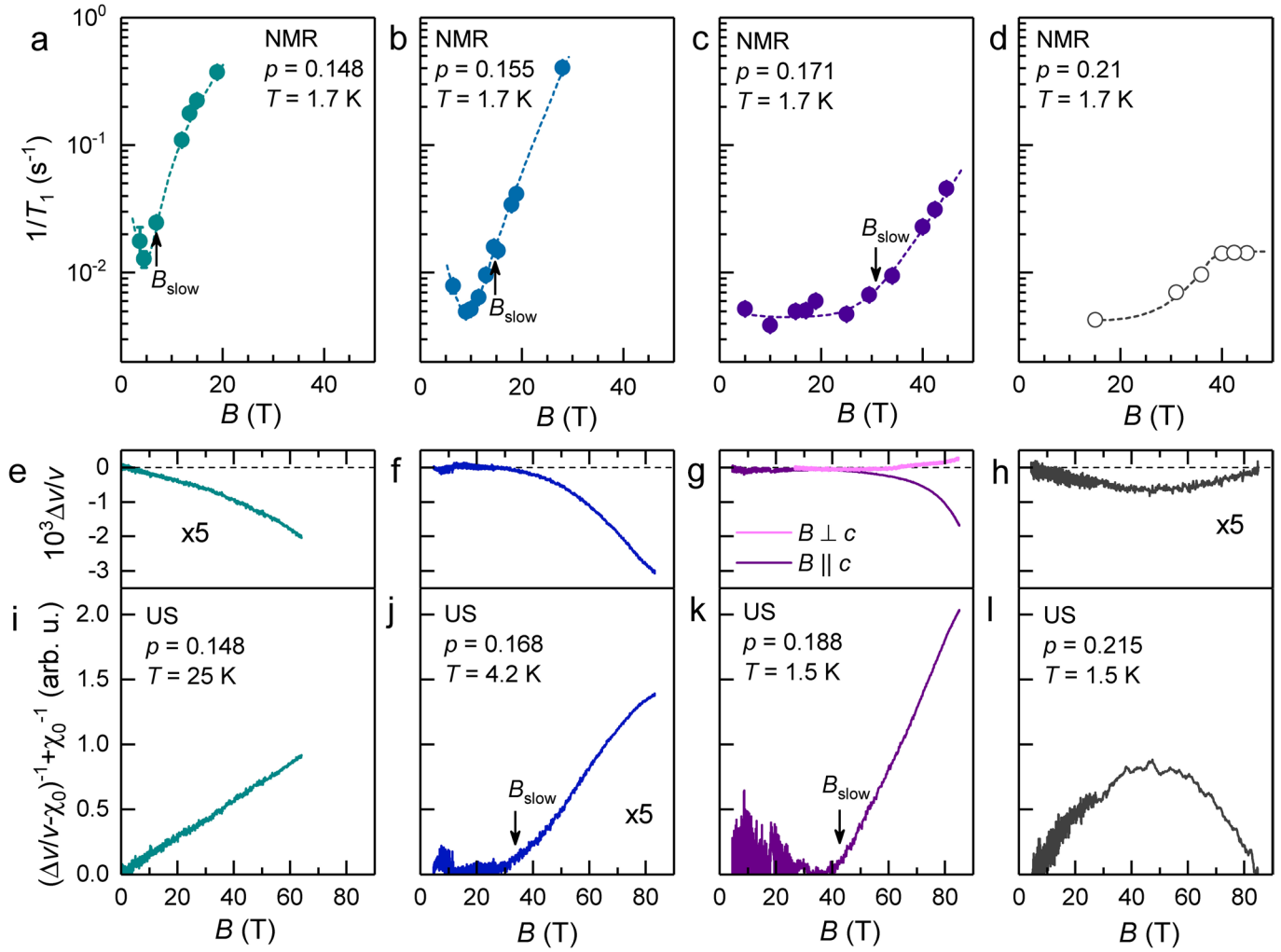


**Extended Data Fig. 3 | Field dependence of glassy freezing. a–d**, Field dependence of $^{139}$La $1/T_1$ at $T = 1.7$ K for different doping levels. The minimum at low fields arises from the balance between an increase of $1/T_1$ upon increasing $B$ (field-induced spin freezing) and a frequency effect ($1/T_1$ decreases with increasing NMR frequency, itself proportional to $B$ – see Methods). Dashed lines are guides to the eye. **e–h**, Field dependence of the sound velocity for different doping levels. In contrast to NMR, ultrasound is measured at constant frequency as a function of field. For each sample with a doping level $p < p^*$, the field dependence is plotted at a temperature where $\Delta v/v$ decreases upon cooling, *that is* for $T \geq T_{min}$ (see Fig. 1). For $p = 0.215$, $\Delta v/v$ is plotted at the lowest $T$ achieved during the experiment. For $p < p^*$ and field $B \parallel c$, $\Delta v/v$ is almost field independent at low fields and above a doping-dependent onset field $B_{slow}$, it shows a strong $1/B$ dependence, highlighted in panels **i–l**. For $B \parallel (110)$ (panel **g**), $\Delta v/v$ shows no softening, and only increases up to 84 T. This highlights that the field effect arises from competition with superconductivity. **i–l**, Inverse field dependent sound velocity $(\Delta v/v - \chi_0)^{-1} + \chi_0^{-1}$, where $\chi_0$ is a doping-dependent constant ($\chi_0 = 0.5 \times 10^{-3}$ for $p = 0.148$, $\chi_0 = 2.2 \times 10^{-3}$ for $p = 0.168$, $\chi_0 = 0.3 \times 10^{-3}$ for $p = 0.188$ and $\chi_0 = 0.4 \times 10^{-3}$ for $p = 0.215$). For $p < p^*$, $(\Delta v/v - \chi_0)^{-1}$ is linear as a function of $B$ for $B > B_{slow}$ (pointed by arrows), with $B_{slow}$ increasing with doping, as shown in Fig. 4. At doping level $p = 0.168$ and for $T = 4.2$ K, $(\Delta v/v - \chi_0)^{-1}$ deviates from linearity for $B > 70$ T, which probably signals the proximity to spin freezing. For $p \approx 0.21$, both the weak field induced softening (**h**,**i**) and the field dependence of $1/T_1$ (**d**) stop at about 40 T, a field value consistent with the upper critical field $B_{c2}$ (Supplementary Fig. 2). The field dependence below 40 T is explained by the suppression of superconductivity in both cases.

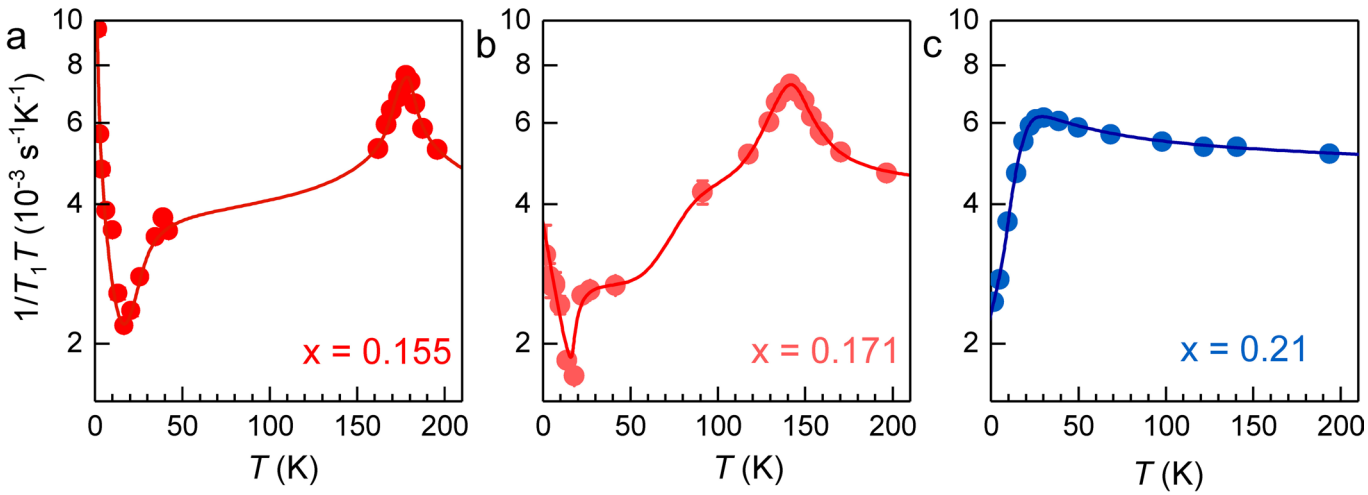


**Extended Data Fig. 4 | Contrasting NMR $T_1$ data below and above $p^* = 0.19$. a–c**, Temperature dependence of $^{139}$La $1/T_1T$ in a field of 15 T for different doping levels. The peak in $1/T_1T$ around 180 K (x = 0.155) and 140 K (x = 0.171) is due to the tetragonal-to-orthorhombic structural transition (electric-field gradient fluctuations contributing to the nuclear relaxation through quadrupolar interaction), the drop below 40 K (all samples) is due to superconductivity and the low $T$ upturn is due to glassy slowing down. This latter is not observed for $x = 0.21$. Also, for this $x = 0.21$ sample, the $T$ dependence in the normal state as well as the large residual $1/T_1T$ value in the $T = 0$ limit are both due to the structural transition at $T \approx 6$ K (that is, the relaxation peak produced by electric-field gradient fluctuations becomes very broad). Lines are guides to the eye.

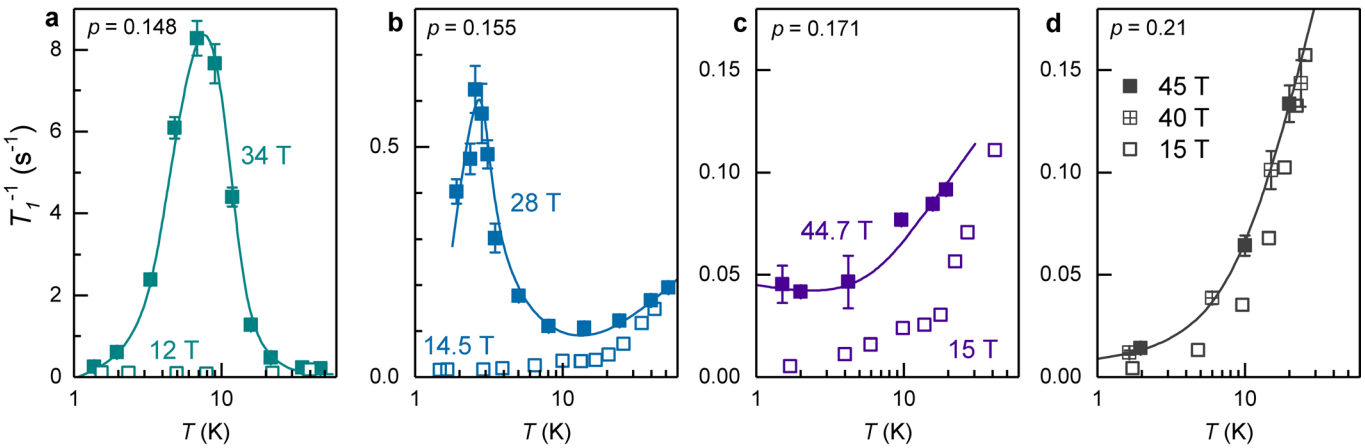


**Extended Data Fig. 5 | $1/T_1$ data *vs.* *T*.** Data (same as in Fig. 3 but not divided by *T*) are shown at selected values of the magnetic fields for each sample. Error bars are s.d. from fits of the nuclear-magnetization recoveries to a stretched-exponential form (see Methods). Lines guide the eye through the highest-field data.

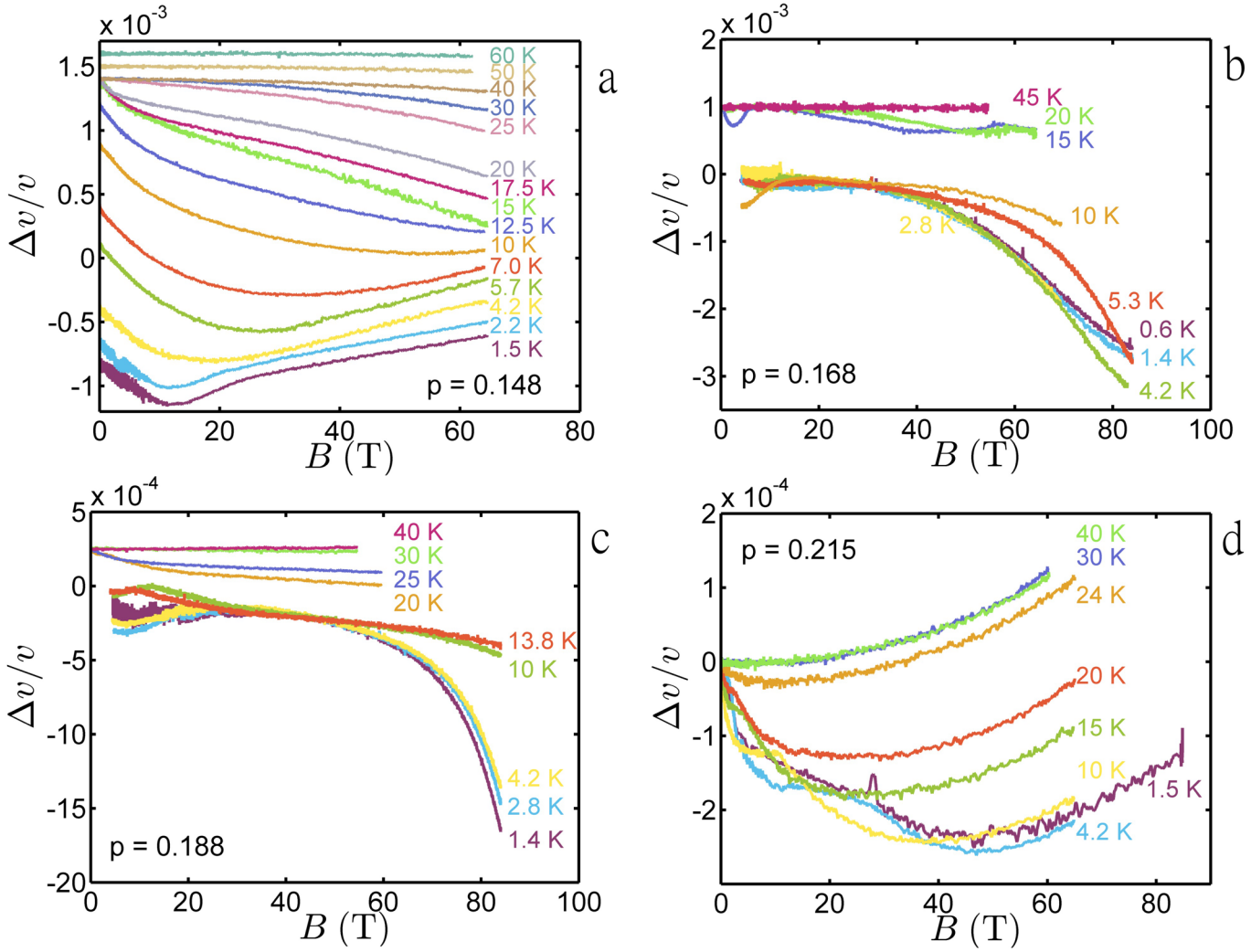


**Extended Data Fig. 6 | Pulsed field sound velocity data at all doping levels. a–d**, Field dependence of the sound velocity, $\Delta v/v(B)$, at different temperatures for $p = 0.148$ (panel a), $p = 0.168$ (panel b), $p = 0.188$ (panel c) and $p = 0.215$ (panel d). The data were obtained at the following measurement frequencies: $f$=225 MHz ($p = 0.148$), $f = 172$ MHz ($p = 0.168$), $f = 187$ MHz ($p = 0.188$) and $f = 244$ MHz ($p = 0.215$). Curves are shifted vertically for clarity. All data presented here are from the downsweep part of the magnetic field pulse. From those data, cuts at constant magnetic field are made in order to obtain the temperature dependence of the field induced sound velocity.

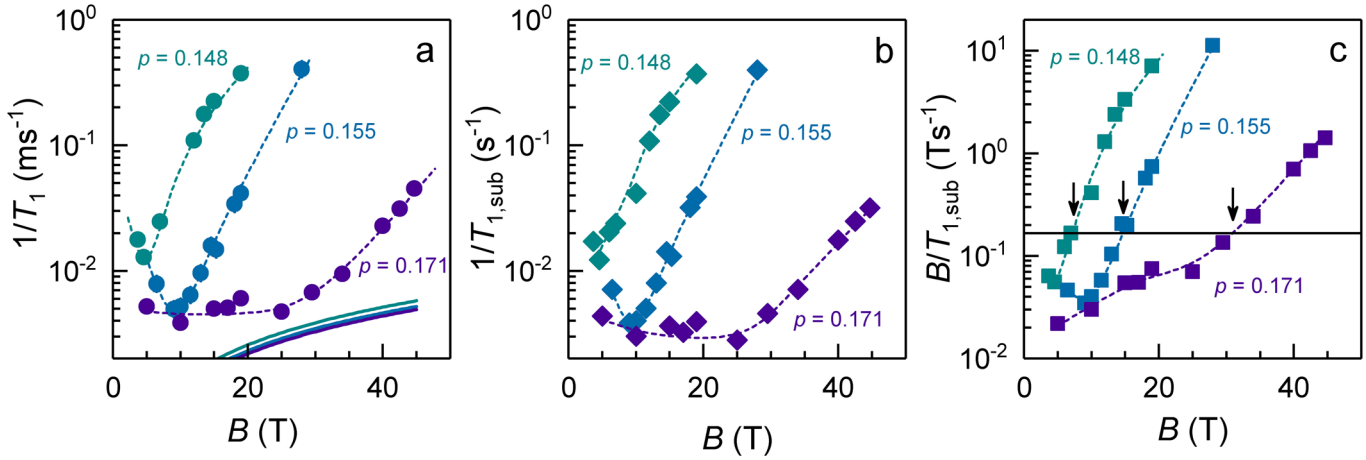


**Extended Data Fig. 7 | Determination of the field scale $B_{slow}$ in NMR data. a**, Field dependence of $^{139}$La $1/T_1$ at $T = 1.7$ K for different doping levels. The minimum at low fields arises from the balance between an increase of $1/T_1$ upon increasing $B$ (field-induced spin freezing) and a frequency effect ($1/T_1$ decreases with increasing NMR frequency, itself proportional to $B$). Lines represent the estimated field dependence of the superconducting background (see Supplementary Fig. 3). **b**, Relaxation rate $1/T_{1,\,sub}$ after subtraction of the superconducting background. **c**, $B/T_{1,sub}$ values. The multiplication by $B$ accounts for the $1/B$ dependence of $1/T_1$ (see Methods). The $B_{slow}$ value for each sample (marked by arrows) is determined from the criterion $B/T_{1,\,sub} = 0.166$ T s$^{-1}$, chosen so as to match neutron scattering results, namely $B_{slow} = 7$ T for $x = 0.148$ (see Methods). Dashed lines are guides to the eye.

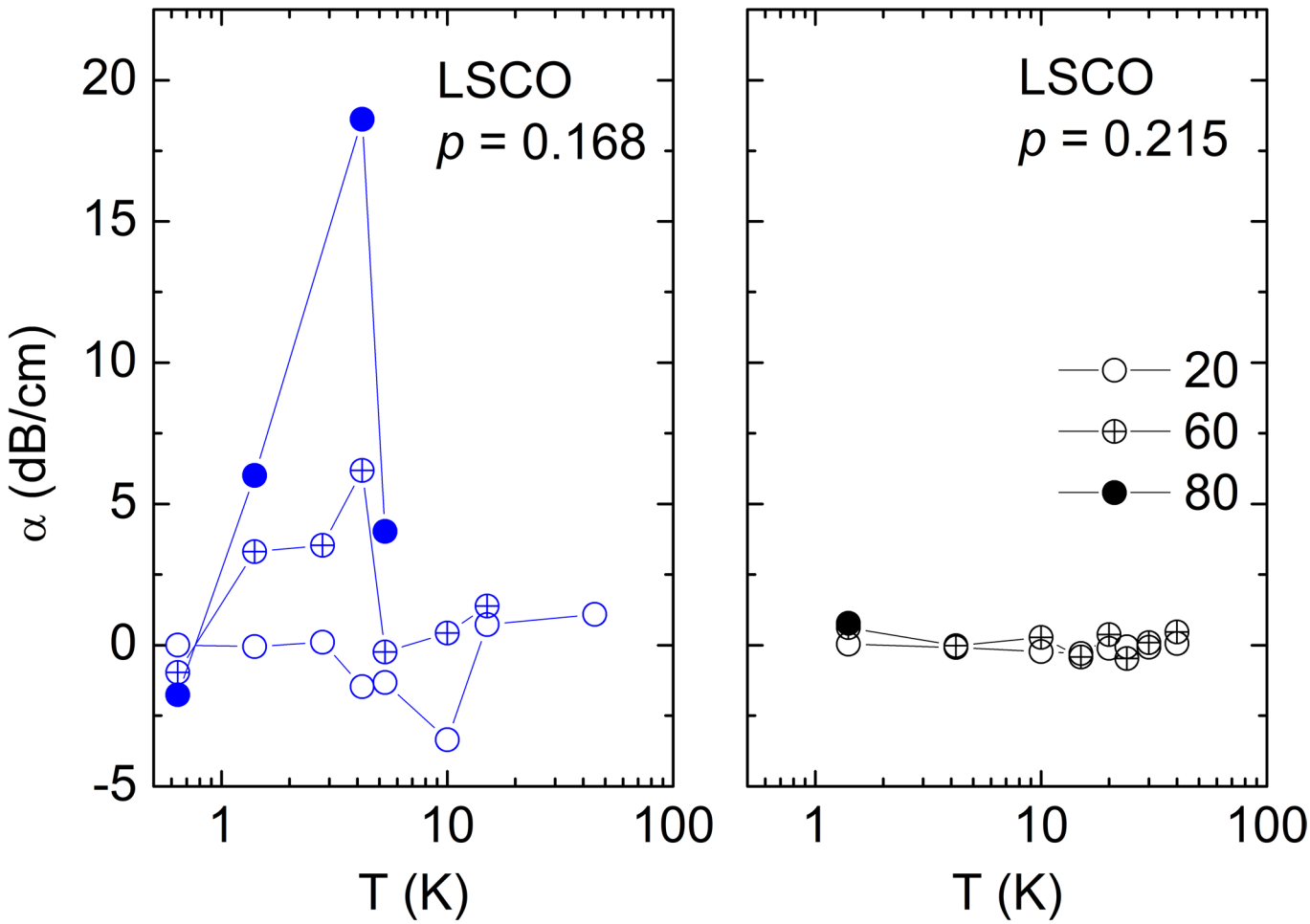


**Extended Data Fig. 8 | Ultrasound attenuation across $p^*$.** In canonical spin glass systems, the slowing down of magnetic fluctuations produces a peak in the ultrasound attenuation α[25]. The origin of this peak is similar to that of the NMR relaxation rate $1/T_1$ peak: when the condition $\omega_{US}\,\tau_c = 1$ is satisfied, a peak develops and defines the freezing temperature at the ultrasound time scale. In the left panel we show such an attenuation peak for our sample with $p = 0.168$, that clearly develops in high fields. This is further evidence that a slowing down, and a freezing, of magnetic fluctuations occur in high field in this sample. In the right panel we show the ultrasound attenuation measured in our sample with $p = 0.215 > p^*$. At this doping level no attenuation peak is observed up to the highest field achieved during the experiment. This confirms the absence of freezing in this sample.

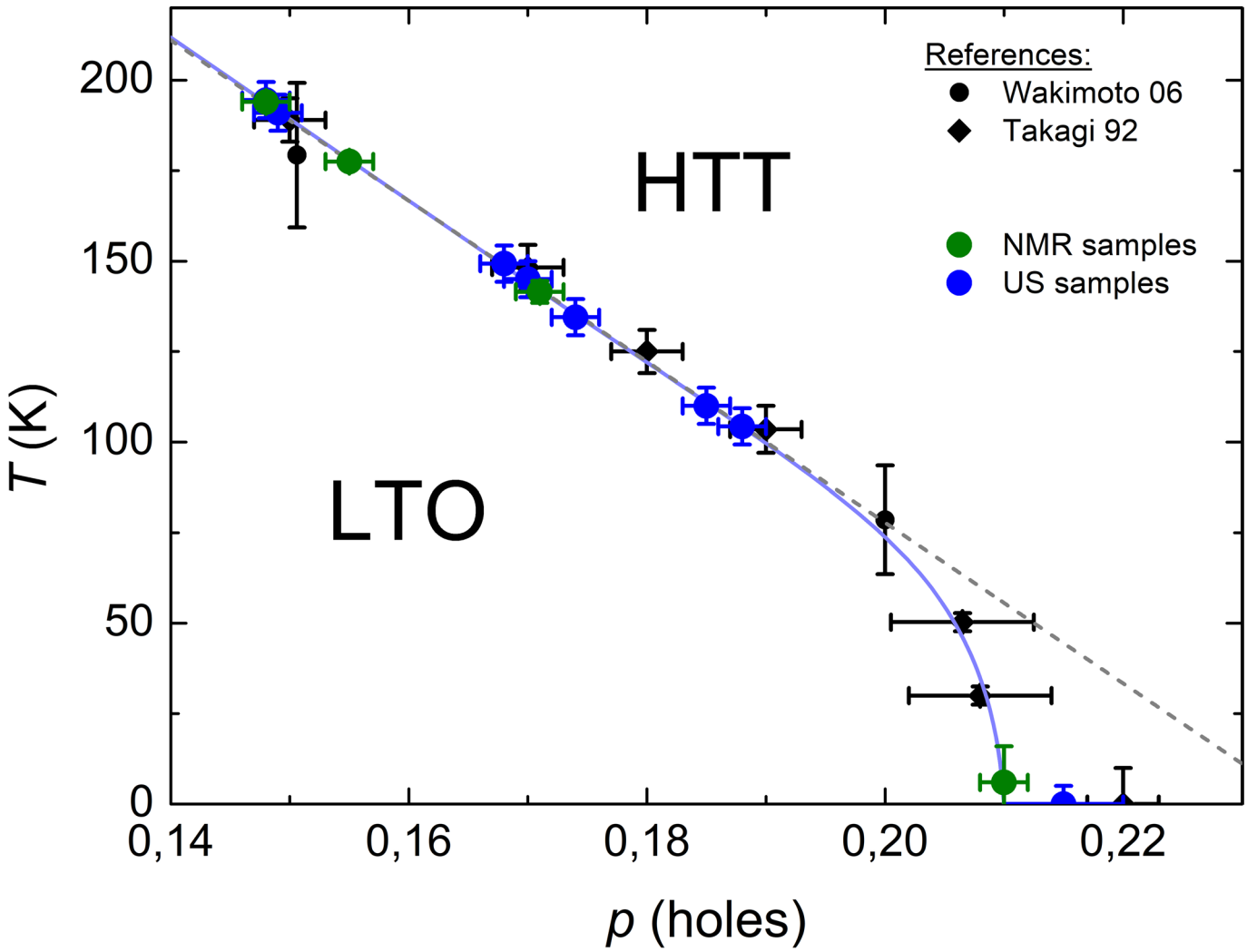


**Extended Data Fig. 9 | Studied samples and their structural transition.** High temperature tetragonal (HTT) to low temperature orthorhombic (LTO) transition temperature $T_{st}$ of NMR (green) and US (blue) samples plotted as a function of doping. The doping of the NMR and US samples is evaluated by comparing $T_{st}$ with original published data shown as black symbols[50,51], as indicated in the legend. For $p \leq 0.188$, we used the simple linear relation $T_{st}(p) = 522 - 2221 \times p$ (dashed line) to extract the doping of our samples. The continuous line is a guide to the eye that indicates a critical doping of $p \approx 0.21$ for the structural transition.

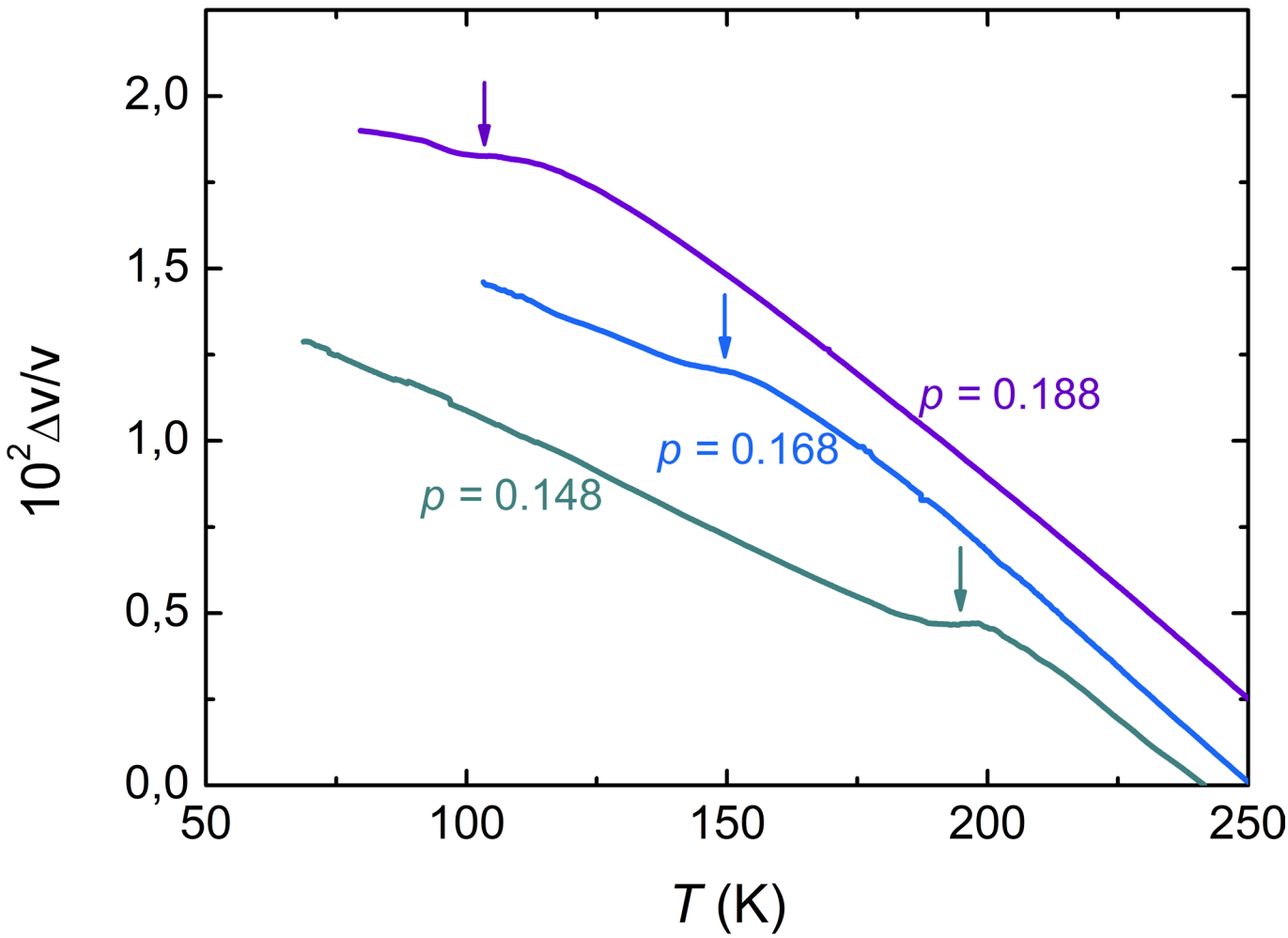


**Extended Data Fig. 10 | Structural transition HTT-LTO observed in sound velocity.** Sound velocity of the mode $(c_{11}-c_{12})/2$ shows a plateau at $T_{st}$, signaling the high temperature tetragonal (HTT) to low temperature orthorhombic (LTO) phase transition, in agreement with previous report[54]. Arrows indicate $T_{st}$ for each doping. For the sample $p = 0.215$ no sign of the structural phase transition is seen down to $T = 7$ K and we therefore used $T_c$ to determine the hole doping of this sample.